# Performance of Artificial Neural Network and Modified Gravitational Search Algorithm Models to Predict Vibration Response of Geocell Reinforced Based Weak Sand

**\* S. Jeyanthi, R.Venkatakrishnaiah, K.V.B. Raju**
*Bharath Institute of Higher Education and Research, Chennai, Tamil Nadu, India.*
*\*Corresponding Author Email: jeyanthinandha@gmail.com*

**Abstract.** *The use of a fast evolving artificial intelligence technology (AIT) to forecast the vibration response of maritime soil based on geocells is explored in this research. The vibration response is represented by an indicator called peak particle velocity (PPV). For the purpose of predicting PPV, the artificial intelligence techniques Artificial Neural Network (ANN) and Modified Gravitational Search Algorithm (MGSA) are employed. To create the dataset for the model, a number of field vibration tests were first performed over the geocell-reinforced beds. PPV variation was investigated by varying the test variables—footing embedment, dynamic load, infill material modulus, width, and depth of geocell mattress placement—during the test performed. The various statistical indicators were determined in order to evaluate the prediction performance of a constructed model. Plate load results on geocell-reinforced foundation beds have been used to validate the proposed hybrid ANN-MGSA model. High accuracy and consistency were found when the findings of the ANN-EHO, JSA, MOA, and RNN method were compared, particularly at predicted and actual resolution levels. A parametric sensitivity has also been examined in order to better understand the behaviour of geocell-reinforced structures.*
**Keywords:** *Soil reinforcement, Geocell reinforced soil foundation, Peak particle velocity (PPV), Confinement and bearing capacity, ANN-MGSA, JSA, MOA, RNN and ANN-EHO.*

## 1.INTRODUCTION

In the field of geotechnical engineering, the idea of soil reinforcement is widely applied. The idea first emerged when metallic cell reinforcements were used in geotechnical constructions, and more recently, synthetic reinforcements have been used [1-3]. Due to their efficiency, tensile resistance, durability, affordability, and ease of application in general for the improvement of weak ground supporting a variety of constructions, geosynthetic materials have been used extensively in practice on foundations, road embankments, and soft soil in recent decades [4]. Early in the 1980s, high density polyethylene or polypropylene copolymer sheet sheets were ultrasonically welded together to create the revolutionary geosynthetic material known as geocell, a three-dimensional mesh construction. The shear strength of coarse soil may be significantly increased by the geocell's lateral limit, which will increase the soil's bearing capacity or halt desertification. Geocells offer greater overall strengths, stable chemical characteristics, and significant flexibility when compared to typical geosynthetics [5-7]. Due to cell confinement and the transfer of stresses to the underlying soil, the geocell also avoids excessive displacements of the infilled soil. The "mattressing" effect, a combined result of the geocell and its fill, enables the reinforced soil to transfer loads to its subgrade much more evenly [8], which contributes to the previously mentioned improvements in bearing capacity, stiffness, and displacement reductions. These advantages are particularly noticeable when used to soft subgrades. The most recent advancement in geosynthetics is geocell reinforcement [9]. It is a three-dimensional, polymeric, honeycomb-like structure of cells joined at joints that is largely reinforced by dirt enclosing all of its surfaces. Additionally, geocells stop possible failure planes and drive them deeper into the foundation soil due to their stiffness. As a result, the failure plane experiences a greater surcharge loading, leading to an increase in load bearing capacity [10].

Numerous studies have already examined the value of the geocells as surface confinement layers and as reinforcement layers. By Tabatabaei et al. [11], who also utilised the full-scale wheel and plate loading approach, dredged sand was used as subsoil. The backfill was reinforced with geocells with a variety of cover layers in order to create an appropriate layered system that complies with the deflection criteria and rutting restrictions (well-graded gravel and dredged sand). Geosynthetic reinforcement layers have been demonstrated by Singh et al. [12] as a method of strengthening the subgrade soil of unpaved roadways. At the midpoint, one-third, and one-fourth of the height of the CBR specimen from

the top surface of the soil in the CBR mould, the thin unit of reinforcement has been applied. A method for calculating the load means of distribution over a geocell layer utilising a non-contact digital image correlation approach has been developed by Gedela et al. [13]. The picture was examined using the Digital Image Correlation (DIC) tool, which produced movement matrices and outlines. The results show that the weight is distributed equally throughout the foundation soil by the geocells. It was found that the height and roughness of the geocell had an impact on the dispersion angle. A number of extensive repeated load model studies have been published by Rayabharapu et al. [14]. To comprehend the overall behavior of reinforced unpaved roads, several load experiments on dense sand layers covering weak sub-grades with and without geocell reinforcement were carried out. The thick sand layer's height was adjusted in accordance with the heights of the geocell mattress being utilized, while the weak subgrade's height was consistently maintained.

For the case of a geocell-reinforced bed supporting a vibration source that might cause harmonic excitation, suggested hybrid ANN-MGSA models are applied in the current work to build the PPV prediction equation. This work stands out as the first of its type in that it attempts to forecast the PPV response of a geocell reinforced bed supporting the vibration source by constructing, evaluating, and proposing hybrid ANN-MGSA models. The database was initially created through field vibration experiments over the geocell reinforced bed. PPV prediction models were created using a field test database. On Chennai's East Coast Road, in a place called Palavakkam, were found the ingredients for the granular poor sand. The predictive performance of both models is compared against an unidentified dataset generated from further field vibration testing in order to determine which PPV prediction model is the best.

## 2. Proposed Methodology

**Weak Sand:** The sand utilized in this study was readily accessible East coast road sand from Palavakkam, which is located near Chennai, India. To remove organic matter like grass roots and other plants, the sand was cleansed. Direct shear tests were performed on models made at relative densities (RD) of 40% and 70% in line with ASTM D 3080/D 3080M-11.The friction angle of soil is stated to be 28° and 31.4° for qualified densities of 40 percent and 70 percent [15]. The results revealed that the uniformity coefficient (Cu) and coefficient of curvature (Cc) were 2.21 and 0.97, respectively. The Unified Soil Classification System (USCS) classifies the soil as poorly graded sand (SP) (ASTM D 2487-06).

**Geocell:** The geocell was represented as a compact, pressurized cylinder made of a linear elastic material with perfect adhesion to the surrounding soil and filling across the whole range of stress and deformation examined (Fig. 1). This leads to complete strain compatibility between the geocell and the soil under operational loads and strains without relative sliding between them, which is a plausible hypothesis for the interaction among geocells replacements and grounds.
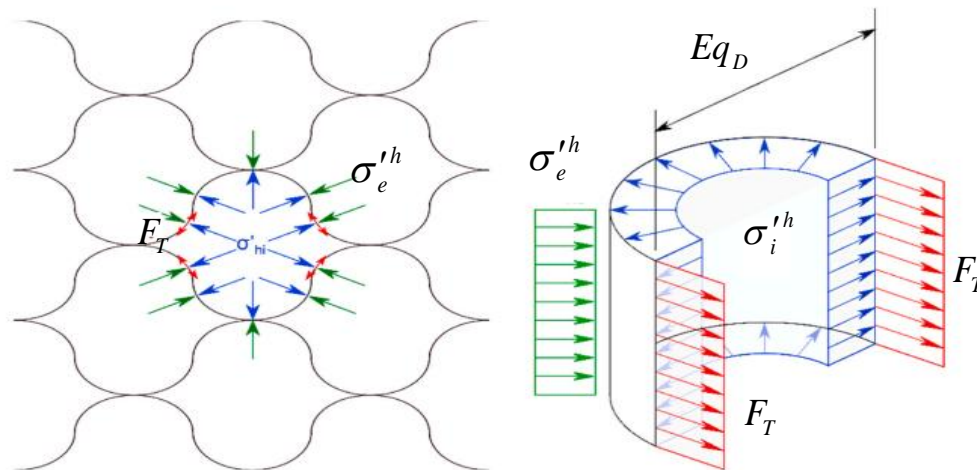


**FIGURE 1.** Internal balance of the soil layer strengthened by geocells

It was supposed that each cell's structure (the geocell wall) was in charge of maintaining its internal horizontal equilibrium. In other words, the cell walls balance the horizontal stresses that are created within each cell after subtracting them from the horizontal forces external to the cell as follows:

$$F_T = \frac{\left(\sigma_i'^h - \sigma_e'^h\right) * Eq_D}{2} \qquad (1)$$

Where $\sigma_i'^{th}$ the internal horizontal stress in the cell, $\sigma_e'^{th}$ is the exterior horizontal stress in the cell, and $F_T$ represents the tensile strain on the cell wall (layup pressure) [16]. The equivalent cell diameter is calculated using the element cell area of a geocell ($A_{GCE}$) as the corresponding equation.

$$Eq_D = \sqrt{\frac{4_{A_{GCE}}}{\pi}} \tag{2}$$

**Objective Function of the proposed method:** The weak sand's stability is improved in this step using the hybrid ANN-MGSA optimization parameter, which is also employed to improve the appearance of the proposed Geocell. Here, the main goal of the suggested hybrid ANN-MGSA approach is to reduce the form characteristic, which is distinct in equation (3) from a scientific perspective,

$$Obj = FF = \begin{cases} P_{\min}^e, S_{\min}^e \\ S_{Ps}^{\max} \end{cases} \tag{3}$$

Where, $P_{\min}^e$ and $S_{\min}^e$ are the minimization of error value of pressure and settlement and $S_{Ps}^{\max}$ is the maximization of stability of the poor sand respectively.

**Controlling of Geocell-Reinforced Soil Foundation Parameters Using Proposed Technique:** This article explains the suggested method for adjusting the specifications of a geocell-reinforced soil foundation dependent on the quality of the soil. The output performance of the suggested system is significantly influenced by the bad soil parameter. The MGSA is used to build the training dataset to enhance the ground soil learning process of the ANN, and in this controlling section, ANN is used to generate the controlling pressure, bearing capacity, density, and peak value velocity. Here is a quick explanation of everything.

**ANN-based Control poor soil parameters:** One artificial intelligence (AI) technology that relies on the training and testing process is the neural network. In this part, an ANN with input, hidden, and output layers was typically taken into account. Here, the MGSA method is used to build the training dataset for ANN depending on the best outcome. Equation (4) gives the network's output training dataset,

$$\begin{bmatrix} (WS_{bc}^{11}, WS_p^{11}.WS_s^{11}) & (WS_{bc}^{12}, WS_p^{12}.WS_s^{12}) & \cdots & (WS_{bc}^{1n}, WS_p^{1n}.WS_s^{1n}) \\ (WS_{bc}^{21}, WS_p^{21}.WS_s^{21}) & (WS_{bc}^{22}, WS_p^{22}.WS_s^{22}) & \cdots & (WS_{bc}^{2n}, WS_p^{2n}.WS_s^{2n}) \\ \vdots & \vdots & \vdots & \vdots \\ (WS_{bc}^{n1}, WS_p^{n1}.WS_s^{n1}) & (WS_{bc}^{n2}, WS_p^{n2}.WS_s^{n2}) & \cdots & (WS_{bc}^{nm}, WS_p^{nm}.WS_s^{nm}) \end{bmatrix} = \begin{bmatrix} v_{out}^*(1) \\ v_{out}^*(2) \\ \vdots \\ v_{out}^*(n) \end{bmatrix} \tag{4}$$

An ANN can offer a statistical connection between multivariate interfaces after training. Equation (5) is used to compute the neuron's output $(Y_i)$,

$$Y_i = \phi(net_i) = \phi\left(\sum_{j=1}^{N} wt_{ij}x_j + \theta_i\right) \tag{5}$$

Here, $\theta_i$ represent the bias of $i^{th}$ neuron, $\phi(\bullet)$ represents the activation function of the layers, $wt = wt_{ij}$ is the matrix of the connection weights between the input and hidden neurons, $v = v_{jk}$ the output and hidden neurons, and both. The input for the neurons in the layer below comes from the output of one neuron. Let the input pattern and the intended yield of the $m^{th}$ output layer neuron make up the training set. Equation (6) represents the error associated with the output neuron once the desired output has been determined,

$$err(n) = v_{out}^*(n) - v_{out}^*(n) \tag{6}$$

Then the training process is given as equation (7),

$$TP_E = \frac{1}{2}\sum_n \left(err(n)\right)^2 \tag{7}$$

Equation (8) describes a rule for continuously updating the weights,

$$wt(n+1) = wt(n) - \eta\left(\frac{\partial TP_E}{\partial wt}\right) \tag{8}$$

Here, $\eta$ represents the learning rate, $n$ is the iteration index, $wt(n+1)$ is the new weight and $w$ is the old weight. The results indicate that weights are crucial to the computation process and may be seen from several angles [17]. Given that

each new learning process begins with the weights that were established during the prior learning process, this operation is repeated for all of the impending learning data.
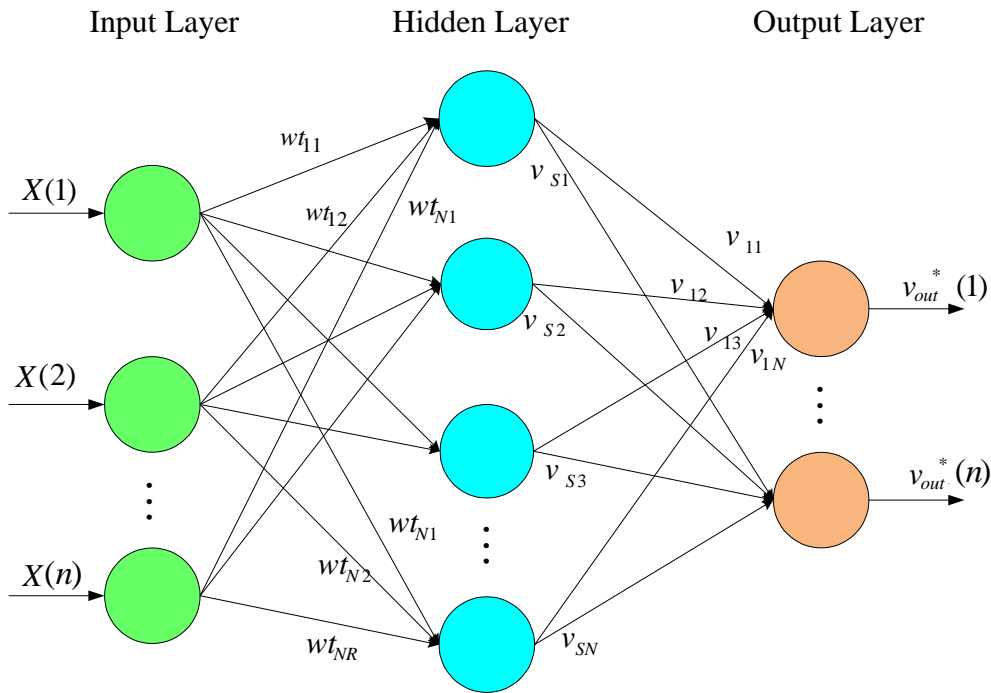


**FIGURE 2.** The testing structure of ANN

Figure 2 shows the proposed neural network's organisational structure for estimate. The neurones are represented by the circles in the network. In order to optimize the learning process, the performance of the ANN is enhanced by selecting the optimal training dataset using the MGSA [18]. When the error is below a predetermined threshold or after a predetermined number of iterations, the neural network simulator software ends during the iterative process of training the network. The MGSA training dataset construction, which is displayed in the next section, was then applied to the recommended system.

**Modified GSA Based Training Dataset Generation:** The creation of training datasets using the GSA searching strategy is detailed in this section. One of the most recent heuristic algorithms, the GSA was created using Rashedi et alphysical .'s principles as inspiration [19]. In MGSA, a collection of agents known as masses are employed to find the best solution in accordance with Newtonian principles of motion and gravity. In order to enhance the ANN's learning process, the training dataset is selected using the MGSA approach. Minimizing the disparity between the current value of the power parameters and their former value is the MGSA's primary purpose. The fitness is then described using an equation (9),

$$fit = \min\left(WS_{bc}, WS_p.WS_s\right) = \min\begin{bmatrix} WS_{bc} - WS_{bc}^{l-1} \\ WS_p - WS_p^{l-1} \\ WS_S - WS_s^{l-1} \end{bmatrix} \qquad (9)$$

The data set is formed by the bearing capacity components $WS_{bc}$, the pressure components $WS_p$ and $WS_S$ the settlements components. The previous values of the bearing capacity components are described as $WS_{bc}^{l-1}$, the pressure components are denoted as $WS_p^{l-1}$ and the settlements components $WS_s^{l-1}$ based on the variation of the bearing capacity, pressure and settlements parameters, the reference poor sand parameter is produced from the output of the MGSA. At the beginning the input agents are bearing capacity, pressure and settlements parameters are described as $X = WS_{bc}, WS_P, WS_S$. Each mass has three characteristics in MGSA, including location, inertial mass $M_i(t)$, active gravitational mass $M_{aj}$, and passive gravitational mass $M_{pi}$. A fitness function is used to specify the location of the mass equal to the problem's solution as well as its gravitational and inertial masses. The position of a system is stated at the start of the procedure with the dimensions of the search space supplied as equation (10),

$$X_i = (X_i^1,..., X_i^d,..., X_i^n) \text{ For } i = 1,2,...,n \qquad (10)$$

Here, $n$ the problem's spatial dimension is $d^{th}$ defined, $X_i^d$ together with the $i^{th}$ agent's location inside it. The following equation contains the random generated agents (11),

$$X_i^d = \begin{bmatrix} (WS_{bc}^{11}, WS_p^{11}.WS_s^{11}) & (WS_{bc}^{12}, WS_p^{12}.WS_s^{12}) & \dots & (WS_{bc}^{1n}, WS_p^{1n}.WS_s^{1n}) \\ (WS_{bc}^{21}, WS_p^{21}.WS_s^{21}) & (WS_{bc}^{22}, WS_p^{22}.WS_s^{22}) & \dots & (WS_{bc}^{2n}, WS_p^{2n}.WS_s^{2n}) \\ \vdots & \vdots & \vdots & \vdots \\ (WS_{bc}^{n1}, WS_p^{n1}.WS_s^{n1}) & (WS_{bc}^{n2}, WS_p^{n2}.WS_s^{n2}) & \dots & (WS_{bc}^{nm}, WS_p^{nm}.WS_s^{nm}) \end{bmatrix} \quad (11)$$

The solution's agents are initially defined at random, and the equation (12) for the gravitational force that arises $t$ when a $i$ mass acts on another mass $j$ is based on Newton's theory of gravity,

$$F_{ij}^d(t) = G(t) \frac{M_i(t) * M_j(t)}{R_{ij} + \varepsilon} * \left(X_j^d(t) - X_i^d(t)\right) \quad (12)$$

Here, $\varepsilon$ is a tiny constant, $R_{ij}(t)$ is the Euclidian distance between, $i$ and $j$ objects, and $M_i$ is the mass of the object $i$, $M_j$ the mass of the object $j$, $G(t)$ the gravitational constant at time $t$, defined as equation (13),

$$R_{ij}(t) = \left\| X_i(t), X_j(t) \right\|_2 \quad (13)$$

Equation (14), $F_i^d(t)$ is used to compute the overall force exerted on the agent $i^{th}$,

$$F_i^d(t) = \sum_{j \in kbest, j \neq i}^{N} rand_j \left(F_{ij}^d(t)\right) \quad (14)$$

Where $rand_j$ is a sequence of numbers between [0, 1] and $kbest$ is the collection of initial $K$ agents with the highest fitness value and largest mass. The rule of motion is applied directly to the calculation of $t$ time in the $d^{th}$ dimension to get the $i^{th}$ agent's acceleration [20]. According to this equation, it is inversely proportional to the mass of the agent and proportionate to the force applied on it. $a_i^d(t)$ expressed as an equation (15),

$$a_i^d(t) = \frac{F_i^d(t)}{M_i(t)} \quad (15)$$

The search method based on this concept may also be used to determine an agent's future speed and location. An agent's next velocity is defined as a component of its current velocity added to its current rising velocity. As a result, the subsequent position and subsequent velocity of an agent can be recorded as having been obtained after condition (16) and (17),

$$V_i^d(t+1) = rand_i V_i^d(t) + a_i^d(t) \quad (16)$$

$$X_i^d(t+1) = X_i^d(t) + V_i^d(t+1) \quad (17)$$

Where, $V_i^d(t)$ and $X_i^d(t)$ the velocity and location of an agent at $t$ a given moment in a $d$ dimension. It is intended to give the search a randomized component. Equation (18), which initializes at random at the beginning and decreases with time to manage search accuracy, represents the gravitational constant $(G)$. $G$ is a function of time $(t)$ and beginning value $(G_0)$,

$$G(t) = G(G_0, t) = G_0 e^{-\alpha \frac{t}{T}} \quad (18)$$

Where $t$ is the current iteration, $T$ is the total number of iterations, and $\alpha$ is a user-specified constant. Using fitness assessment, the agent masses are calculated. An agent's influence over the solution it represents increases with its bulk, according to research [19]. It is noteworthy that a heavier mass has a stronger draw on power and moves more slowly according to Newton's laws of gravity and motion. In accordance with equation (19) and (20),

$$M_{ai} = M_{pi} = M_{ii} = M_i \text{ Where } i = 1, 2, ..., N$$

$$m_i(t) = \frac{fit_i(t) - worst(t)}{best(t) - worst(t)} \quad (19)$$

$$M_i(t) = \frac{m_i(t)}{\sum_{j=1}^{N} m_j(t)} = V_{out}^{ref} \tag{20}$$

Where, $fit_i(t)$ denotes the agent's $i$ fitness value at time $t$, $best(t)$ and $worst(t)$ in the population, respectively, identify the agent with the best and worst fitness pathway. A minimization issue is presented in this equation (21) and (22)

$$best(t) = \min_{j \in \{\{1, \dots m\}} fit_j(t) \tag{21}$$

$$worst(t) = \max_{j \in \{\{1, \dots m\}} fit_j(t) \tag{22}$$

In order to tackle the optimisation problem using MGSA, each agent is first assigned to a certain position in the search space that provides a solution to the issue at every unit of time [20]. The agents are then retrieved and their subsequent locations are calculated based on velocity and position. Finally, the best fitness value from the output of the MGSA method is chosen, constructed into a matrix, and the best dataset for training the ANN is chosen. Figure 3 displays the flow diagram for the suggested approach.
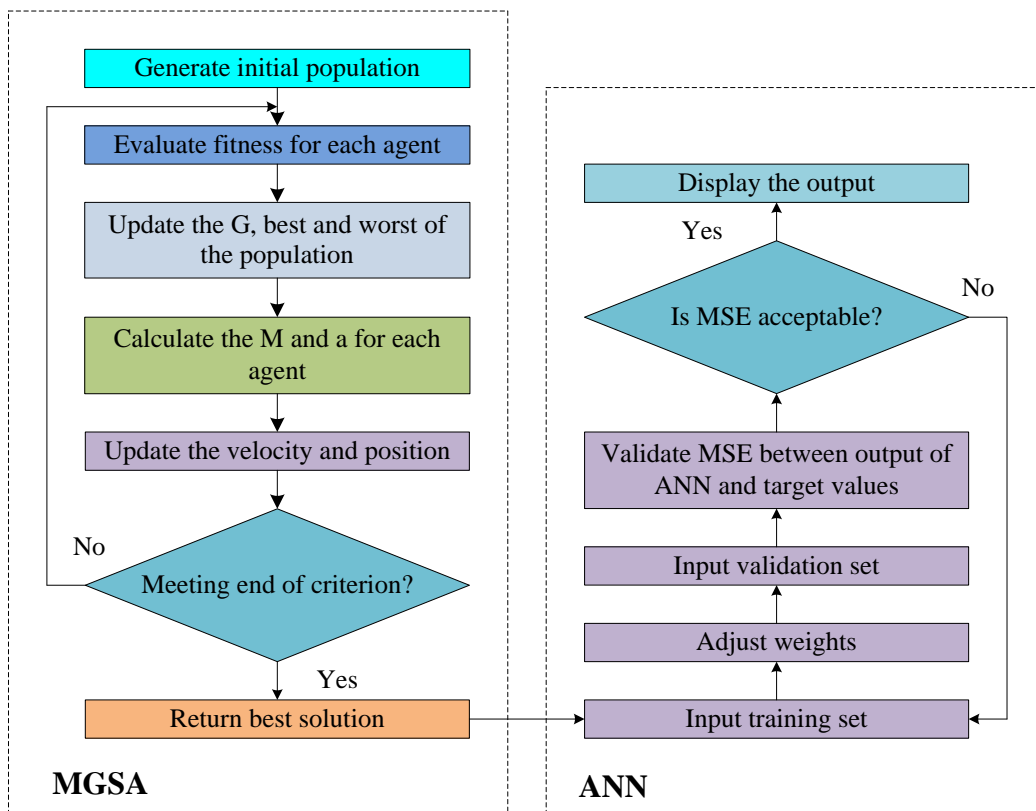


**FIGURE 3.** The flow diagram of the MGSA

After finished above process, the MGSA is ready to give the training dataset for the ANN. The attained training dataset is utilized to train the ANN. Using this data set, the network is trained and output of the network is denoted as $v_{out}^*$. Based on the output of the network, the proposed method is established the optimal control pulses of the voltage source converter based on the grid parameter variations. Then the proposed method is implemented in the Matlab platform and the results were analyzed in the following section 3.

# 3. RESULTS AND DISCUSSION

By defining dimensionless improvement factors linked to the final bearing capacity and settlement settlements of the foundation, the improvement of the bearing capacity and settlement settlements of the foundation is stated in order to evaluate the performance of sand foundations reinforced with geo cells. The Matlab 7.10.0 (R2021a) and an Intel (R) Core (TM) i5 CPU with 4GB RAM platform power the geocell-reinforced sand foundations. The new system was put to the test, and its processing settings were compared to a variety of methods, such as the ANN-Elephant Herding

Optimization (EHO), jellyfish search algorithm (JSA), Mayfly Optimization Algorithm (MOA) and Recurrent Neural Network (RNN) models, in order to validate its performance. Table 1 lists the Geocell's input settings.

**TABLE 1.** Properties of geocell

| Soil properties | Values |
|---|---|
| Polymer | Polyvinyl Chloride |
| Cell height (mm) | 75 |
| Diagonal size (along length) | 60 |
| Diagonal size (along width) | 265 |
| Number of cells (/m²) | 0.03 |
| Mass per unit area (gm/cm²) | 2.75 |
| Cell depth (cm) | 5 |
| Strip thickness (micron) | 250 |
| Coefficient of thermal expansion/ppm $^0$C | <80 |
| % Open area | 15 |
| Short term yield strength/kN m$^{-1}$ | 21.5 |

**Table 2.** The implementation parameters of the proposed MGSA-ANN technique

| ANN | | GSA | |
|---|---|---|---|
| **Parameters** | **Values** | **Parameters** | **Values** |
| Number of Inputs | 2 | Number of Agents | 10 |
| Number of hidden layers | 10 | Maximum iterations | 5 |
| Number of outputs | 1 | The dimension of the best function | 2 |
| Number of epoch | 1000 | Minimum flag | 500 |
| | | Elitist check | 10 |

**Uncertainty analysis:** Wilmot's Index of Agreement (WI), Mean Absolute Percentage Error (MAPE), Mean Absolute Percentage Error (RMSE), Mean Absolute Percentage Error (MAPE), Mean Absolute Percentage Error (RMSE), coefficient of correlation ($R^2$), and mean absolute error (MAE) were all calculated to evaluate the performance of the final selected architecture for the proposed ANN-MGSA (i.e., testing information that the network hasn't encountered throughout the training). Equations (23) to (27) are used to compute the values of MAE (mean absolute error), RMSE (root-mean-square error), and R for the training and testing portions.

Five indicators were used to assess how well the suggested machine learning models performed:

**RMSE:** The standard errors between predicted values and actual values can be represented using RMSE. The algorithm is defined as being given in Eq and is said to be more exact the smaller the RMSE represents (23).

$$RMSE = \sqrt{\frac{1}{n}\sum_{i=1}^{n}\left(O_S^i - P_S^i\right)^2} \tag{23}$$

**Correlation Coefficient (R):** R measures how strongly the measured values and the variation in forecasted values are related. The R value varies from - 1 to 1, where - 1 denotes a completely inverse correlation and - 1 denotes a completely inverse correlation. The definition of R is given in Eq. (24)

$$R\left(P^i, O^i\right) = \frac{cov\left(P^i, O^i\right)}{\sqrt{var\left[P^i\right] * var\left[O^i\right]}} \tag{24}$$

**Mean Absolute Percentage Error (MAPE):** A dimensionless measure called MAPE may be used to rate a model's ability to anticipate outcomes. The greater the model's derived predictive performance, the closer MAPE is to 0. Equation represents the MAPE definition (25).

$$MAPE = \frac{100\%}{n}\sum_{i=1}^{n}\frac{\left|P_S^i - O_S^i\right|}{P_S^i} \tag{25}$$

**Coefficient of Determination ($R^2$):** $R^2$ measures how closely the anticipated value resembles the actual value. R2 is between 0 and 1. The perfect match between the anticipated value and the actual value is shown by an R2 of 1. Equation (26) displays R2's definition.

$$R^2 = 1 - \frac{\sum_{i=1}^{n}\left|P_S^i - O_S^i\right|}{\sum_{i=1}^{n}\left|O_S^i - O_S\right|} \tag{26}$$

***Wilmot's Index of Agreement (WI):*** WI, which ranges from 0 to 1, is a standardised index to measure the prediction efficacy of established models. A WI of 0 shows no match at all, whereas a WI of 1 shows complete agreement between predicted values and actual values. Equation (27) displays the WI definition.

$$WI = 1 - \frac{\sum_{i=1}^{n}\left|P_S^i - O_S^i\right|}{\sum_{i=1}^{n}\left|O_S^i - O_S\right|} \tag{27}$$

Where, $O_S^i$, $P_S^i$ and $n$ stands for $i^{th}$ the observed value of settlement, $i^{th}$ the anticipated value of settlement, and the quantity of data samples, respectively.

**TABLE 3.** Comparison analysis of proposed models and existing methods based on statistical indices

| Statistical index | ANN | ANN-EHO | JSA | MOA | RNN | Proposed ANN-MGSA |
|---|---|---|---|---|---|---|
| **RMSE** | 0.813 | 0.586 | 0.512 | 0.481 | 0.457 | 0.394 |
| **MPAE (%)** | 30.5 | 25.6 | 23.45 | 19.54 | 17.69 | 12.21 |
| **Efficiency** | 0.963 | 0.974 | 0.98 | 0.987 | 0.989 | 0.99 |
| **R²** | 0.891 | 0.904 | 0.924 | 0.937 | 0.953 | 0.963 |
| **WI** | 0.897 | 0.885 | 0.905 | 0.933 | 0.947 | 0.956 |
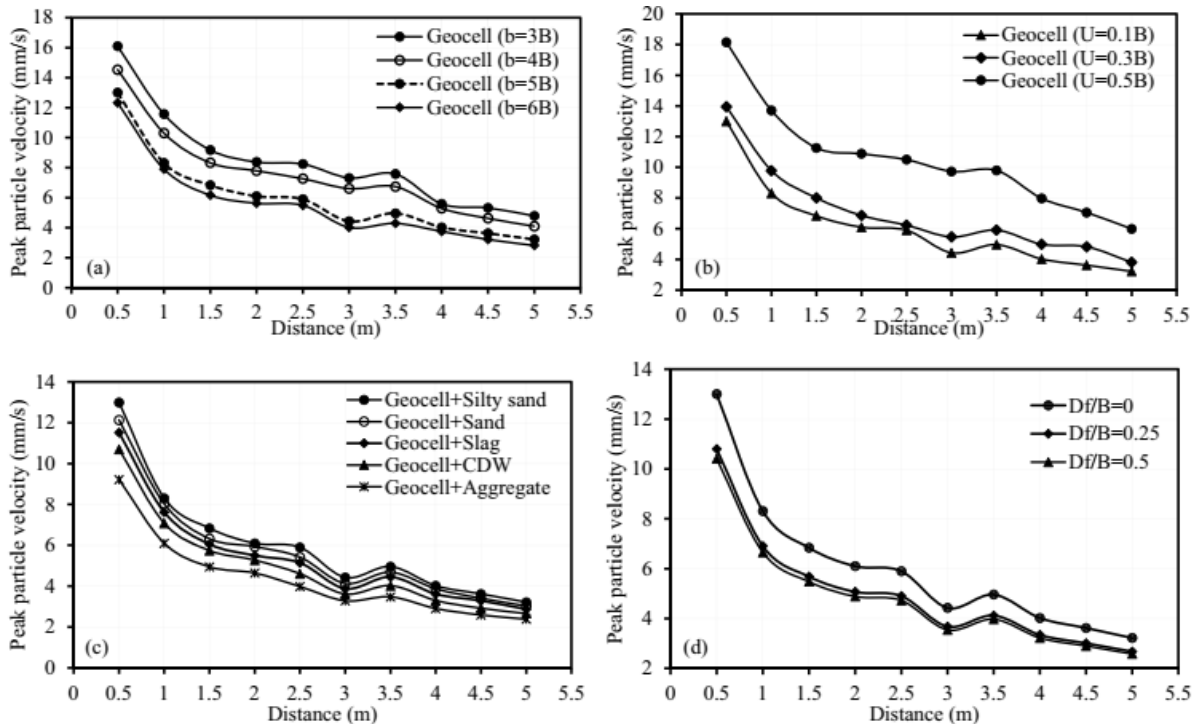


**FIGURE 4.** Geocell reinforced bed with PPV variation for (a) cushion width, (b) geocell deployment depth, (c) infill substance stiffness, and (d) footing embedment

Regarding geocell width, installation depth, infill type, and footing embedment, Fig. 4a–d depicts the PPV variation of the geocell reinforced bed. Figure 4a shows the effect of the geocell mattress's breadth on PPV. It was discovered that when the geocell's diameter increased, the pace at which PPV decreased did as well. The geocell's capacity to stop the motion of produced vibration is indicated by the declining trend of PPV. The PPV decline rate was minimal beyond the 5B geocell width (B is the thickness of an actual mass). As a result, it was found that the geocell width of 5B was perfect for effectively reducing PPV. Fig 4 (b) depicts how the geocell's placement depth affects the PPV. The depth at which the

geocell (U) was buried beneath the concrete block was shown to be inversely linked to the percentage reduction in PPV response. It illustrates that a key element in lowering vibration velocity is the depth at which a geocell is placed. Geocell deployment at 0.1B of depth is advised for the significant reduction of PPV. There may be a chance for reflection of produced vibrations when geocell installation depth is increased. Figure 4c displays the PPV variation for various infill material moduli. The geocell pockets were filled with five different materials, whose elastic moduli ranged from 28.3 to 60 MPa. No of the distance, PPV values were much lower in the case of the aggregate infilled material than - other materials. It reveals that PPV mitigation is improved when employing an infill material with a higher modulus. The greatest decrease in PPV was caused by an improvement in the geocell reinforced bed's damping ratio as a result of the infill material's greater elastic modulus. Therefore, a new method to improve the screening efficiency of geocell reinforced beds is to increase the modulus of the infill material. The effect of footing embedment on PPV in the presence of a geocell reinforced substrate is shown in Fig. 4d.
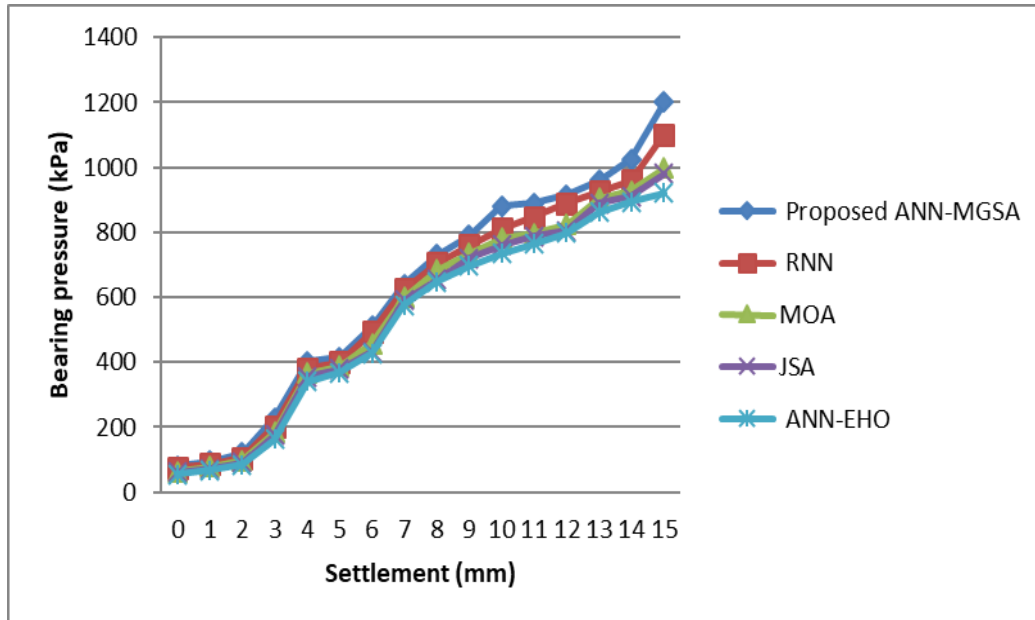


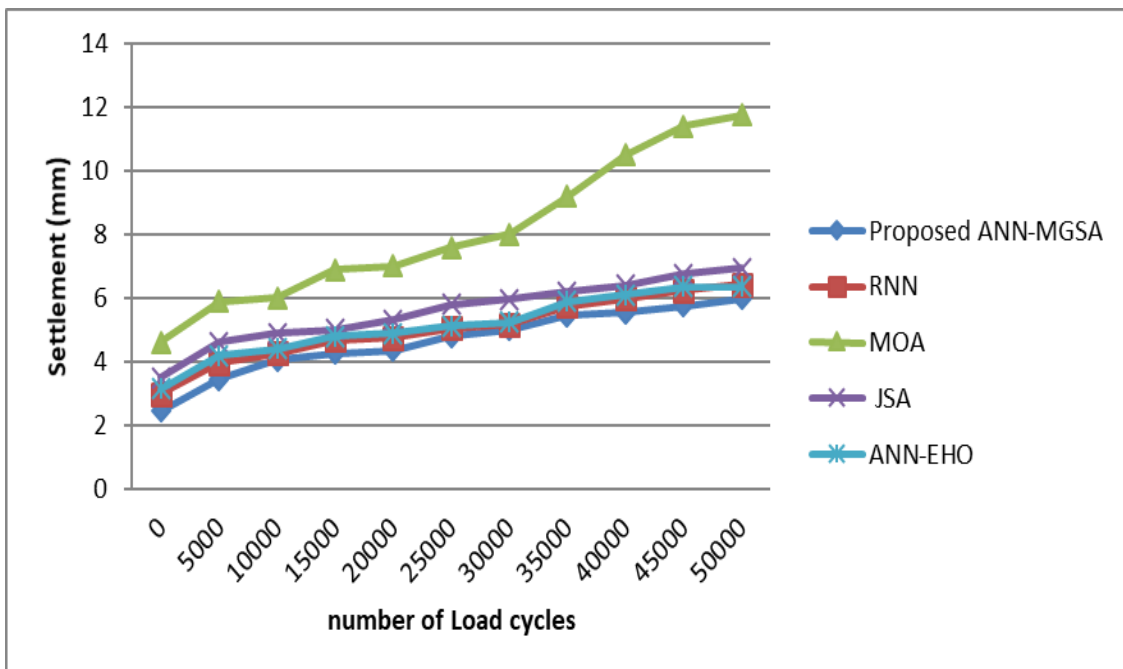**FIGURE 5.** Bearing pressure-settlement curve for different methods of the geo cell



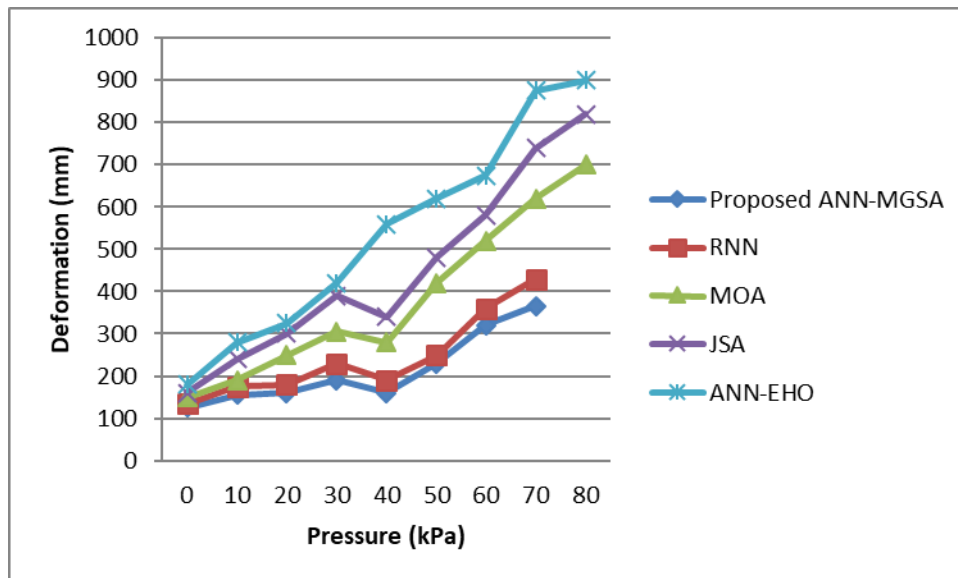**FIGURE 6.** Results of settlement with number of load repetitions

**FIGURE 7.** Comparison analysis of deformation at the foundation with 100 mm thick base

In Fig. 5, the pressure-settlement behaviours of three distinct situations are contrasted. With an increase in geocell height, the bearing capacity of the geocell reinforced foundation bed improved. similar observational techniques utilising experimental research. The footing load will be spread across more space as the geocell's height rises. Typical information on settlement variation for a 53 mm thick granular subbase layer with several geosynthetic reinforcement layer types is shown in Figure 6. The findings shown that the poor sand's initial modulus is rather large; as settlement increased with the number of cycles, the modulus value reduced; and eventually, towards the end of 18000 cycles, the modulus value stabilized at a constant value. As demonstrated in Figure 7, the ultimate bearing capacity of lime stone aggregate bases reinforced with geocells rises 1.2 times over unreinforced bases for 100 mm height geocells. The overall bearing capacity augmentation factor was also increased by 68%. When the suggested method course was properly compacted, the results demonstrate a considerable improvement in the performance of the proposed ANN-MGSA technique using Geocell compared to other methods such as ANN-EHO, JSA, MOA and RNN respectively.

# 4. CONCLUSION

In this article, proposed a hybrid Artificial Neural Network- Modified Gravitational Search Algorithm approach was suggested to examine the geocell-reinforced sand's improvement effect under static stress. When reinforcing material with a range of specifications is used to build geocells, the impact of the mechanical features of the geocell on the bearing pressure-settlement response of the impoverished sand is investigated. Increased bearing pressure and a percentage reduction in settlement for real settlement levels and the strain capacity grade are two metrics used to evaluate the effectiveness of geocell-reinforced sand. According to the comparison analysis, the suggested technique MOA based on geocell reinforced soil foundation performs better than other models like ANN-EHO, JSA, MOA and RNN.

➤ The constant stiffness number of the soil, the secant modulus of the geocell, the thickness of the geocell layers, and the total number of geocell layers all have a significant and nonlinear impact on the response of pressure settlement in reinforced and unreinforced situations.

➤ The results confirmed that a foundation strengthened with geocells regularly outperforms a foundation without one.

➤ The numerical outcome demonstrates that when the number of geosynthetic layers, inclination stiffness, and height of geocell layers rise, the growth rate in absorption over a certain foundation solution decreases. As a result, the suggested technique may hold promise for geocell applications in infrastructure and transport engineering, particularly for the design of roads and pavements that are constructed effectively and economically.

➤ Strong coefficient of efficiency (E) values for the algorithms demonstrated that any geotechnical engineering issue may be modeled using a hybrid ANN-MGSA optimizer with the appropriate inputs and outputs.

# REFERENCES

[1]. Hegde, A. "Geocell reinforced foundation beds-past findings, present trends and future prospects: a state-of-the-art review." Construction and Building Materials 154 (2017): 658-674.

[2]. Zhou, Huabao, and Xuejun Wen. "Model studies on geogrid-or geocell-reinforced sand cushion on soft soil." Geotextiles and Geomembranes 26.3 (2008): 231-238.

[3]. Zhang, Ling, et al. "Bearing capacity of geocell reinforcement in embankment engineering." Geotextiles and Geomembranes 28.5 (2010): 475-482.

[4]. Biswas, Arghadeep, and A. Murali Krishna. "Geocell-reinforced foundation systems: a critical review." International Journal of Geosynthetics and Ground Engineering 3.2 (2017): 1-18.

[5]. Dash, Sujit Kumar, and Mukul Chandra Bora. "Improved performance of soft clay foundations using stone columns and geocell-sand mattress." Geotextiles and Geomembranes 41 (2013): 26-35.

[6]. Hegde, A. "Geocell reinforced foundation beds-past findings, present trends and future prospects: a state-of-the-art review." Construction and Building Materials 154 (2017): 658-674.

[7]. Saride, Sireesh, Vijay K. Rayabharapu, and Suraj Vedpathak. "Evaluation of rutting behaviour of geocell reinforced sand subgrades under repeated loading." Indian Geotechnical Journal 45.4 (2015): 378-388.

[8]. Pokharel, Sanat K., et al. "Investigation of factors influencing behavior of single geocell-reinforced bases under static loading." Geotextiles and Geomembranes 28.6 (2010): 570-578.

[9]. Sherin, K. S., S. Chandrakaran, and N. Sankar. "Effect of geocell geometry and multi-layer system on the performance of geocell reinforced sand under a square footing." International Journal of Geosynthetics and Ground Engineering 3.3 (2017): 1-11.

[10]. Sitharam, T. G., and A. Hegde. "Design and construction of geocell foundation to support the embankment on settled red mud." Geotextiles and Geomembranes 41 (2013): 55-63.

[11]. Tabatabaei Aghda, Seyed Taha, Ali Ghanbari, and Gholamhosein Tavakoli Mehrjardi. "Evaluating the applicability of geocell-reinforced dredged sand using plate and wheel load testing." Transportation Infrastructure Geotechnology 6.1 (2019): 21-38.

[12]. Singh, Meenakshi, Ashutosh Trivedi, and Sanjay Kumar Shukla. "Strength enhancement of the subgrade soil of unpaved road with geosynthetic reinforcement layers." Transportation Geotechnics 19 (2019): 54-60.

[13]. Gedela, Ramesh, et al. "Assessment of load distribution mechanism in geocell reinforced foundation beds using Digital Imaging Correlation Techniques." Transportation Geotechnics 31 (2021): 100664.

[14]. Rayabharapu, Vijay Kumar, and Sireesh Saride. "Geocell reinforced dense sand bases overlying weak sand sub-grades under repeated loading." Ground Improvement Techniques and Geosynthetics. Springer, Singapore, 2019. 285-294.

[15]. Sarkar, Haradhan, and Arghadeep Biswas. "Behaviour of Multi-layered Geocell-Reinforced Soil Embankment." Proceedings of the 7th Indian Young Geotechnical Engineers Conference. Springer, Singapore, 2022.

[16]. Sarkar, Haradhan, and Arghadeep Biswas. "Response of Multilayered Stepped Geocell Reinforcement in Soil Structures." Proceedings of the Indian Geotechnical Conference 2019. Springer, Singapore, 2021.

[17]. Yang, Guangyu Robert, and Xiao-Jing Wang. "Artificial neural networks for neuroscientists: A primer." Neuron 107.6 (2020): 1048-1070.

[18]. Buscema, Paolo Massimo, et al. "Artificial neural networks." Artificial adaptive systems using auto contractive maps. Springer, Cham, 2018. 11-35.

[19]. Olivas, Frumen, et al. "Interval type-2 fuzzy logic for dynamic parameter adaptation in a modified gravitational search algorithm." Information Sciences 476 (2019): 159-175.

[20]. Ebrahimi Mood, Sepehr, and Mohammad Masoud Javidi. "Energy-efficient clustering method for wireless sensor networks using modified gravitational search algorithm." Evolving systems 11.4 (2020): 575-587.